# Organometallic Mixed-Valence Systems. Electronic Coupling through an Alkyndiyl Bridge Incorporating Methylene Groups

Séverine Roué and Claude Lapinte*

*Organométalliques et Catalyse: Chimie et Electrochimie Moléculaire, UMR CNRS 6509, Institut de Chimie de Rennes, Université de Rennes 1, Campus de Beaulieu, F-35042 Rennes, France*

Thierry Bataille

*Laboratoire de Chimie du Solide et Inorganique Moléculaire, UMR CNRS 6511, Institut de Chimie de Rennes, Université de Rennes 1, Campus de Beaulieu, F-35042 Rennes, France*

*Received December 10, 2003*

Downloaded by NAT LIB UKRAINE on July 5, 2009
Published on April 20, 2004 on http://pubs.acs.org | doi: 10.1021/om034359i

The binuclear complexes [Cp*(dppe)FeC≡C−$(CH_2)_x$−C≡CFe(dppe)Cp*] ($x = 3$ (**8a**), $x = 4$ (**8b**)) were prepared by deprotonation of the parent bis(vinylidene) derivatives [Cp*(dppe)-Fe═C═C(H)−$(CH_2)_x$−(H)C═C═Fe(dppe)Cp*] $[PF_6]_2$ ($x = 3$ (**7a**), $x = 4$ (**7b**)). The X-ray crystal structure of **8a** revealed that the metal−metal distance (8.706 Å) is much shorter that the sum of the bond distances of the Fe−Fe assembly (12.24 Å). An X-ray powder diffraction analysis of an amorphous sample shows that the Fe−Fe distance may fall into the wide range 8.50−10.75 Å. The resolved separations between the redox processes in the cyclic voltammograms evidenced the through-bridge interaction between the iron centers and enabled computations of the comproportionation constants ($K_c$) and the molar fractions of the different species $\mathbf{8a}^{n+}$ and $\mathbf{8b}^{n+}$ ($n = 0, 1, 2$) present in solution. The dicationic complexes **8a**$[PF_6]_2$ and **8b**$[PF_6]_2$ were prepared in good yield by oxidation of **8a** and **8b** with 2 equiv of ferrocenium. The IR, Mössbauer, ESR, and UV−vis spectra provided evidence for a small through-bridge interaction between the $Fe^{III}$ sites. The NIR spectroscopy study of the MV complexes **8a**$[PF_6]$ and **8b**$[PF_6]$ clearly shows that through-bridge electron transfer occurs for both compounds, which well obey Hush's theory.

## Introduction

Understanding and control of electron transfer reactions constitute major challenges in science. Electron transfer is one of the most fundamental chemical processes: it occurs in nature to produce inter alia ATP, the source of biological energy. In chemistry, many reactions involving bond breaking and bond formation often proceed through electron transfer mechanisms.[1] At the molecular level, understanding and controlling electron transfer is a key point in the development of molecular electronics.[2] The design of molecular models for molecular electronics is based on the idea that the material between the donor and acceptor plays a major role in promoting the electronic coupling interaction between the redox-active centers.[3] In addition, it has been widely shown that conjugated organic molecules are irreplaceable in the construction of efficient molecular wires.[4−8] Many years ago, it was shown that cyclobutane and heterocyclobutanes are capable of achieving electron delocalization through hyperconjugation.[9,10] A decade later, it was shown that intervalence electron transfer reactions take place between ruthenium atoms of complexes of the type $[(NH_3)_5Ru-(S<>S)-Ru(NH_3)_5][PF_6]$, where (S<>S) represents dithiaspiro bridging ligands.[11] In addition, CNDO/2 calculations for these compounds support a hyperconjugating electron transfer pathway between the ruthenium centers bonded to the terminal sulfur atoms.[12] However, despite several remarkable works, it is less clear for many chemists that through-bond long-distance electron transfer can take place across saturated hydrocarbon bridges.[11−16]

(1) March, J. *Advanced Organic Chemistry*, 4th ed.; John Wiley & Sons: New York, 1992.
(2) Barbara, P. F.; Meyer, T. J.; Ratner, M. A. *J. Phys. Chem.* **1996**, *100*, 13148.
(3) Astruc, D. *Electron Transfer and Radical Processes in Transition-Metal Chemistry*; VCH: New York, 1995.
(4) Aviram, A.; Ratner, M. A. *Chem. Phys. Lett.* **1974**, *29*, 277.
(5) Mujica, V.; Kemp, M.; Ratner, M. A. *J. Chem. Phys.* **1994**, *101*, 6856.
(6) Ward, M. D. *Chem Ind.-London* **1996**, 568.
(7) Joachim, C. *New J. Chem.* **1991**, *15*, 223.
(8) Paul, F.; Lapinte, C. *Coord. Chem. Rev.* **1998**, *178−180*, 427.
(9) Mollere, P. D. *Tetrahedron Lett.* **1973**, *29*, 2791.
(10) Mollere, P. D.; Houk, K. N. *J. Am. Chem. Soc.* **1977**, *99*, 3226.
(11) Stein, C. A.; Lewis, N. A.; Seitz, G. *J. Am. Chem. Soc.* **1982**, *104*, 2596.
(12) Stein, C. A.; Lewis, N. A.; Seitz, G.; Baker, A. D. *Inorg. Chem.* **1983**, *22*, 1124.
(13) Curtiss, L. A.; Miller, J. R. *J. Phys. Chem. A* **1998**, *102*, 160.
(14) Lokan, N.; Paddon-Row, M. N.; Smith, T. A.; La Rosa, M.; Ghiggino, K. P.; Speiser, S. *J. Am. Chem. Soc.* **1999**, *121*, 2917.
(15) Craig, D. C.; Paddon-Row: M. N. *Aust. J. Chem.* **1987**, *40*, 1951.
(16) Closs, G. L.; Carlcatera, L. T.; Green, N. J.; Penfield, K. W. J. R. *J. Phys. Chem.* **1986**, *90*, 3673.

10.1021/om034359i CCC: $27.50 © 2004 American Chemical Society
Publication on Web 04/20/2004

Downloaded by NAT LIB UKRAINE on July 5, 2009
Published on April 20, 2004 on http://pubs.acs.org | doi: 10.1021/om034359i

**Chart 1**

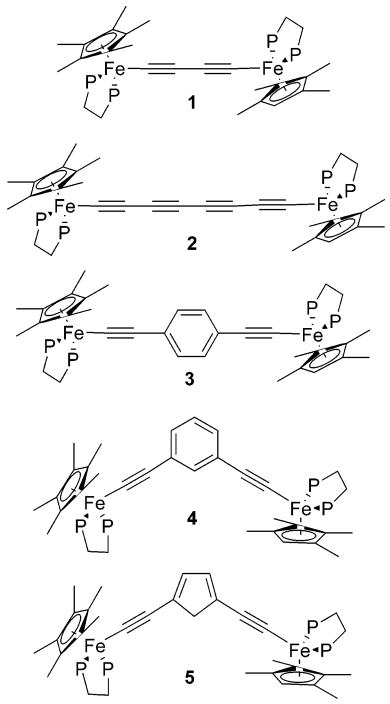


In previous papers we described the synthesis and physical properties of the bis(iron) molecules of general formula [Cp*(dppe)Fe−C≡C−X−C≡C−Fe(dppe)Cp*]-[$PF_6$]$_n$ (X = none (**1**);[17] −C≡C−C≡C− (**2**);[18] 1,4-$C_6H_4$ (**3**);[19] 1,3-$C_6H_4$ (**4**);[20] 2,5-$C_4H_2S$ (**5**);[21] $n$ = 0, 1, 2; Chart 1). All these compounds were isolated as $Fe^{II}-Fe^{II}$, $Fe^{II}-Fe^{III}$, and $Fe^{III}-Fe^{III}$ stable derivatives, and the investigation of their spectroscopic or magnetic properties revealed electronic and magnetic coupling with various strength between the metal ends.[8,22] The mixed-valence (MV) derivatives associated with complexes **1**, **2**, **3**, and **5** are clearly nontrapped class III MV compounds as defined by the Robin and Day classification.[23] In contrast, the *meta* connection of the Cp*Fe(dppe) units through the phenylethynyl rigid spacer in **4** leads to localized organometallic MV complexes. In this complex a rather weak electronic coupling ($V_{ab}$ = 150 $cm^{-1}$) is associated with a weak reaction organization energy ($\lambda$ = 5500 $cm^{-1}$) and a low barrier for the thermal process ($\Delta G^*$ = 4 kcal/mol).[20] To explore the unclear role played by saturated hydrocarbon bridges in mixed-valence (MV) systems we planed the synthesis and study of the organometallic complexes [Cp*(dppe)Fe−C≡C−$(CH_2)_x$−C≡C−Fe(dppe)Cp*][$PF_6$]$_n$ ($x$ = 3 (**8a**$^{n+}$), 4 (**8b**$^{n+}$), $n$ = 0, 1, 2). Comparison of the properties of these compounds with those of **4**$^{n+}$ should contribute to improve the understanding of the ability of the saturated hydrocarbons to convey electrons.

**Scheme 1**

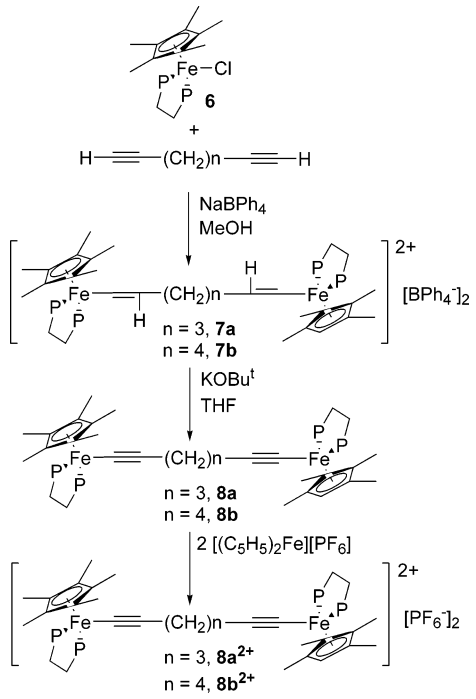


Besides (i) the synthesis of **8a** and **8b**, we also report here (ii) the X-ray crystal structure and the powder diffraction diagram of **8a**, (iii) the analysis of the comproportionation equilibrium between the components of the systems on the basis of electrochemical data, (iv) the synthesis, isolation, and characterization of the diradical dications **8a**[$PF_6$]$_2$ and **8b**[$PF_6$]$_2$, and (v) the full spectroscopic characterization of the MV complexes **8a**[$PF_6$] and **8b**[$PF_6$] in situ generated.

## Results

**1. Synthesis and Characterization of 8a and 8b.** Complexes **8a** and **8b** were prepared in a two-step procedure involving the formation and the isolation of the corresponding vinylidene followed by a double deprotonation as previously described in these series for the preparation of mono- and binuclear alkynyl complexes (Scheme 1).[19,24] Treatment of the commercially available terminal akynes HC≡C−$(CH_2)_n$−C≡CH with 2 equiv of Cp*(dppe)FeCl (**6**) and $NaBPh_4$ in methanol produced after 16 h a dark orange solution, from which the bis(vinylidene) complexes [Cp*(dppe)Fe=C=C(H)−$(CH_2)_x$−(H)C=C=Fe(dppe)Cp*][$PF_6$]$_2$ ($x$ = 3 (**7a**), $x$ = 4 (**7b**)) were isolated as orange powders in 97 and 96% yields, respectively. Traces of mononuclear vinylidene could not be evidenced, indicating that the reactions easily proceed at both ends of the bis(alkynes). The complexes **7a** and **7b** were characterized by the usual techniques (see Experimental Section).

The complexes **7a** and **7b** were readily deprotonated by 2 equiv of KOBu$^t$ in THF at 20 °C, giving the corresponding bis(alkynyl) complexes [Cp*(dppe)FeC≡C−$(CH_2)_x$−C≡CFe(dppe)Cp*] ($x$ = 3 (**8a**), $x$ = 4 (**8b**)) isolated as thermally stable red-orange powders in 90 and 92% yields, respectively. The neutral complexes were characterized by the usual spectroscopies and high-resolution LSI mass spectrometry, while subsequent single-crystal X-ray diffraction data obtained for

(17) Le Narvor, N.; Toupet, L.; Lapinte, C. *J. Am. Chem. Soc.* **1995**, *117*, 7129.
(18) Coat, F.; Lapinte, C. *Organometallics* **1996**, *15*, 477.
(19) Le Narvor, N.; Lapinte, C. *Organometallics* **1995**, *14*, 634.
(20) Weyland, T.; Costuas, K.; Toupet, L.; Halet, J.-F.; Lapinte, C. *Organometallics* **2000**, *19*, 4228.
(21) Le Stang, S.; Paul, F.; Lapinte, C. *Organometallics* **2000**, *19*, 1035.
(22) Paul, F.; Lapinte, C. In *Unusual Structures and Physical Properties in Organometallic Chemistry*; Wrackmeyer, B., Ed.; John Wiley & Sons: London, 2002; p 220.
(23) Robin, M. B.; Day, P. *Adv. Inorg. Chem. Radiochem.* **1967**, *10*, 247.

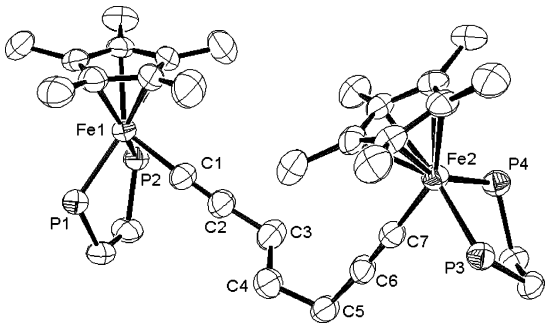


**Figure 1.** Structure of **8a** showing thermal ellipsoids at the 50% probability level.

**8a** also confirmed the proposed structures (Figure 1). The FTIR spectra display the C≡C bond stretching at $\nu$ 2082/2080 and 2080/2080 (Nujol/$CH_2Cl_2$, $cm^{-1}$) for **8a** and **8b**, respectively. The NMR data are in line with the usual features expected for such complexes.[24,25] Notably, in the $^{13}C$ NMR, the alkynyl α-carbon atoms of **8a** and **8b** appear coupled to the two phosphorus atoms of the dppe ligand with a $^3J_{PC}$ coupling constant of 41 Hz (**8a**, $\delta$ 108.7; **8b**, $\delta$ 109.1). In addition, the $\beta$-carbon atoms are observed at $\delta$ 117 for both complexes and the $^4J_{PC}$ coupling of ca. 3 Hz is resolved in the case of **8b**.

**2. X-ray Crystal Structure and Powder Diffraction Pattern of 8a.** No −C− chains incorporating methylene groups between alkynyl fragments with two end-capping organometallic moieties have been structurally characterized to date. The M−C≡C−$(CH_2)_n$−C≡C−M arrangement was only X-ray characterized for M = Si in sterically hindered compounds.[26−29] Crystals of **8a** were grown by slow diffusion of methanol into a $CH_2Cl_2$ solution of **8a**. The unit cell contains two molecules. The molecular structure of **8a** is shown in Figure 1, and the X-ray data conditions are summarized in Table 1. Complex **8a** crystallizes in the triclinic space group $P\bar{1}$. As usually observed for many earlier structures of related piano-stool complexes, the two metal centers clearly adopt pseudooctahedral geometries with bond lengths and angles in previously established ranges.[17,25,30−32] Various data in Table 2 are relevant to results below. For example, the Fe−Cα≡ bonds (1.909(5) and 1.917(5) Å) are longer than analogous iron−C(sp) bonds in the closely related complex [Cp*(dppe)Fe−C≡C−C≡C−Fe(dppe)Cp*] (**1**)[33] (1.884(2) and 1.889(2) Å) but remain shorter than iron−C($sp^3$) in [Cp*(dppe)Fe(CHOMe)][$PF_6$].[34] Interestingly, the lengthening of the Fe−Cα≡ is associated with a small shortening of the Cα≡C$\beta$ bonds (1.204(7) and 1.216(7) Å) with respect to its congener **1** (1.220(4) and 1.221(4) Å).[17] The structural changes observed on the Fe(II) acetylides, albeit weak, are exactly what one would expect from the breaking of the $\pi$-interactions along the iron−iron linkage.[17,25] The bond distances between the central carbon atoms of the bridge (1.506(7) and 1.534(7) Å) are very close to the typical distance generally observed between C($sp^3$) (1.54 Å),[35] whereas the $\sigma$-bonds between C(sp) and C($sp^3$) atoms are shorter (1.481(7) and 1.473(6) Å), but slightly longer than the standard C(sp)−C($sp^3$) distance (1.46 Å).[36,37] The presence of C($sp^3$) in the bridge allows flexibility of the carbon backbone of the linker and the metal−metal distance (8.706 Å) is much

**Table 1. Crystallographic Data for 8a**

| | |
|---|---|
| molecular formula | $C_{79}H_{84}Fe_2P_4$ |
| molecular weight | 1269.04 |
| cryst syst | triclinic |
| space group | $P\bar{1}$ |
| cell dimens | |
| *a*, Å | 8.479(5) |
| *b*, Å | 19.603(5) |
| *c*, Å | 21.125(5) |
| α, deg | 73.641(5) |
| $\beta$, deg | 85.148(5) |
| $\gamma$, deg | 89.585(5) |
| *V*, Å$^3$ | 3357(2) |
| *Z* | 2 |
| $d_{calc}$, g/cm$^3$ (294 K) | 1.256 |
| absorp coeff (mm$^{-1}$) | 0.571 |
| *F*(000) | 1340 |
| cryst dimens (mm) | 1.15 × 0.14 × 0.04 |
| diffractometer | Nonius Kappa CCD |
| radiation (Å) | Mo Kα (0.71069) |
| data collection method | $\omega/2\theta$ |
| $t_{max}$/measure, s | 63 |
| range/indices (*h*,*k*,*l*) | −10, 10; −24, 25; −27, 26 |
| $\theta$ range | 1.01 to 27.14 |
| no. of reflns measd | 41 761 |
| no. of indep reflns | 14 824 |
| obsd data, $I > 2\sigma(I)$ | 5970 |
| no. of variables | 766 |
| $R_{int}$ (from merging equiv reflns) | 0.0165 |
| final *R* | 0.1920 [$R_w$ = 0.1792] |
| *R* indices (all data) | 0.0623 [$R_w$ = 0.1291] |
| GOF | 0.914 |
| largest diff peak and hole, e Å$^{-3}$ | 0.43; −0.48 |

**Table 2. Selected Distances (Å) and Angles (deg) for 8**

| | | | |
|---|---|---|---|
| Fe1−P1 | 2.1661(15) | P1−Fe1−P2 | 85.69(6) |
| Fe1−P2 | 2.1783(15) | P3−Fe2−P4 | 86.34(6) |
| Fe2−P3 | 2.1682(15) | C1−Fe1−sP1 | 85.83(16) |
| Fe2−P4 | 2.1642(15) | C1−Fe1−P2 | 82.62(16) |
| Fe1−C1 | 1.909(5) | C7−Fe2−P3 | 84.84(15) |
| Fe2−C7 | 1.917(5) | C7−Fe2−P4 | 86.14(15) |
| C1−C2 | 1.204(7) | Fe1−C1−C2 | 176.6(5) |
| C2−C3 | 1.481(7) | C1−C2−C3 | 176.9(6) |
| C3−C4 | 1.506(7) | C2−C3−C4 | 115.3(5) |
| C4−C5 | 1.534(7) | C3−C4−C5 | 112.9(5) |
| C5−C6 | 1.473(6) | C4−C5−C6 | 112.4(4) |
| C6−C7 | 1.216(6) | C5−C6−C7 | 176.2(5) |
| Fe1−Cp*[a] | 1.745(5) | C6−C7−Fe2 | 174.3(4) |
| Fe2−Cp*[a] | 1.735(5) | Cp*[a]−Fe1−Fe2Cp*[a] | 14.60(4) |
| Fe1−Fe2 | 8.706(6) | | |

Downloaded by NAT LIB UKRAINE on July 5, 2009
Published on April 20, 2004 on http://pubs.acs.org | doi: 10.1021/om034359i

(24) Connelly, N. G.; Gamasa, M. P.; Gimeno, J.; Lapinte, C.; Lastra, E.; Maher, J. P.; Narvor, N. L.; Rieger, A. L.; Rieger, P. H. *J. Chem. Soc., Dalton Trans.* **1993**, 2575.
(25) Denis, R.; Toupet, L.; Paul, F.; Lapinte, C. *Organometallics* **2000**, *19*, 4240.
(26) Haberhauer, G.; Rominger, F.; Gleiter, R. *J. Chem. Soc., Perkin Trans. 2* **1999**, 947.
(27) Haberhauer, G.; Gleiter, R.; Irngartiner, H.; Oeser, T.; Rominger, F. *J. Chem. Soc., Perkin Trans. 2* **1999**, 2093.
(28) Stahr, H.; Gleiter, R.; Haberhauer, G.; Irngartiner, H.; Oeser, T. *Chem. Ber.* **1997**, *130*, 1807.
(29) Gleiter, R.; Stahr, H.; Stadtmuller, F.; Irngartiner, H.; Pritzkow, H. *Tetrahedron Lett.* **1995**, *36*, 4603.
(30) Le Narvor, N.; Lapinte, C. *J. Chem. Soc., Chem. Commun.* **1993**, 357.
(31) Weyland, T.; Lapinte, C.; Frapper, G.; Calhorda, M. J.; Halet, J.-F.; Toupet, L. *Organometallics* **1997**, *16*, 2024.
(32) Coat, F.; Guillevic, M.-A.; Toupet, L.; Paul, F.; Lapinte, C. *Organometallics* **1997**, *16*, 5988.
(33) Jiao, H.; Costuas, K.; Gladysz, J. A.; Halet, J.-F.; Guillemot, M.; Toupet, L.; Paul, F.; Lapinte, C. *J. Am. Chem. Soc.* **2003**, *125*, 9511.
(34) Roger, C.; Toupet, L.; Lapinte, C. *J. Chem. Soc., Chem. Commun.* **1988**, 713.
(35) Hedberg, K.; Schomaker, V. *J. Am. Chem. Soc.* **1951**, *73*, 1482.
(36) Lerner, R. G.; Dailet, B. P. *J. Chem. Phys.* **1957**, *26*, 678.
(37) Sheehan, W. F.; Schomaker, V. *J. Am. Chem. Soc.* **1952**, *74*, 4468.

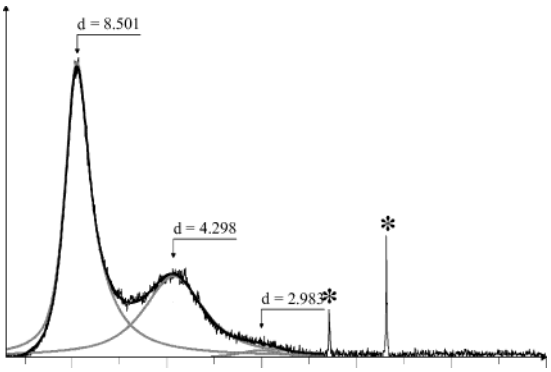


**Figure 2.** X-ray powder diffraction pattern of **8a**, indicating the positions of the fitted lines. * stands for sample holder (NiO).

shorter than the sum of the bond distances of the Fe−Fe assembly (12.24 Å).

To obtain a rough indication of the iron−iron distance in solution, a solid was prepared by removal of the solvent from a concentrated $CH_2Cl_2$ solution of **8a**. X-ray powder diffraction analysis shows that the pattern of the sample is characteristic of a noncrystalline compound (Figure 2). It is known that noncrystalline maxima denote the frequent occurrence of particular interatomic distances in largely disordered substances.[38] These distances are given in only an approximate sense by the Bragg equation,

$$K\lambda = 2x_m \sin \theta_m \qquad (1)$$

where $\lambda$ is the wavelength of the radiation used, $x_m$ is the distance of the largest number of atom pairs separated by a bond length $x$, $\theta_m$ is the angular position of the given peak, and $K$ is a factor derived from the Debye formula.[36] Its value usually falls into the range 1−1.25, depending on the mutual arrangement of the atoms. Figure 2 displays two maxima with a high intensity at 8.501 and 4.298 Å, while a third maximum with a low intensity could be observed at 2.983 Å. From the positions of the two intense peaks, it can be deduced that the second maximum is a harmonic line of the first maximum. According to the scattering power of the heavy atoms involved in **8a**, i.e., Fe ($Z$ = 26) and P ($Z$ = 15), it is assumed that the fitted position of the first peak (8.501 Å) corresponds to the rough distance between the two intramolecular Fe atoms. Similarly, the fitted position of the third maximum (2.983 Å) is in agreement with the P−P bond length within the P−$CH_2$−$CH_2$−P group observed from the crystal structure of the compound. According to eq 1, it can be deduced that Fe−Fe and P−P distances may fall into the wide ranges 8.50−10.75 and 2.98−3.73 Å, respectively.

**3. Cyclic Voltammetry of 8a and 8b.** The initial scans in the cyclic voltammogram of complexes **8a** and **8b** from −1.3 to 1.2 V [vs standard calomel electrode (SCE)] are characterized by two distinct and reversible one-electron waves (Figure 3). This indicates that at the platinum electrode the neutral dimer undergoes two successive one-electron oxidations to yield the mono- and the dications, respectively. Simulation of the cyclic voltammograms allows the determination of the peak potentials given in Table 3. The decrease of the wave separation ($\Delta E°$) from 0.120 to 0.094 when the number of methylene groups increases from 3 to 4 indicates that the two remote iron termini communicate through the bonding.

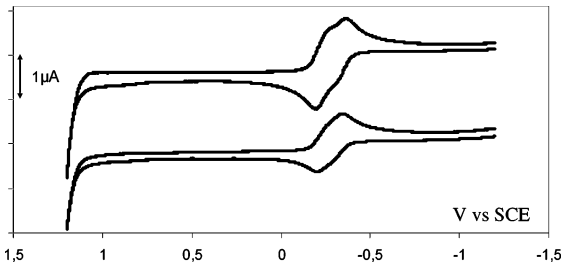


**Figure 3.** Cyclic voltammograms of **8a** (top) and **8b** (bottom) in 0.1 M $n$-$Bu_4N^+PF_6^-$/$CH_2Cl_2$ (Pt electrode; V vs SCE; scan rate 0.100 V/s; 20 °C).

**Table 3. Electrochemical Data for Compounds 8a, 8b, and Closely Related Compounds[a]**

| cmpd | $E°_1$ | $E°_2$ | $\Delta E°$ | $K_c$ | ref |
|---|---|---|---|---|---|
| **8a** | −0.336 | −0.216 | 0.120 | 96 | this work |
| **8b** | −0.32 | −0.24 | 0.094 | 35 | this work |
| **4** | −0.100 | −0.225 | 0.13 | 130 | 27 |
| **9**[b] | −0.11 | | | | 8 |

[a] Potentials in $CH_2Cl_2$ (0.1 M [$Bu_4^nN$][$PF_6$]; 20 °C, Pt electrodes, sweep rate 0.100 V $s^{-1}$) are given in V vs SCE; the ferrocene−ferrocenium couple (0.460 V vs SCE) was used as an internal calibrant for the potential measurements. [b] Compound **9** is Cp*(dppe)FeC≡C−$Bu^t$.

The comproportionation constant $K_c$ relative to the equilibrium in eq 2 can be calculated from the wave splitting for compounds **8a** and **8b** (Table 3).[8]

$$Fe^{II}-C\equiv C-(CH_2)_x-C\equiv C-Fe^{II} + [Fe^{III}-C\equiv C-(CH_2)_x-C\equiv C-Fe^{III}]^{2+} \rightleftharpoons 2\,[Fe^{III}-C\equiv C\text{-}(CH_2)_x-C\equiv C-Fe^{III}]^{+} \qquad (2)$$

From these data, the molar fractions of the different species in solution were calculated. There were found to be 0.085, 0.830, and 0.085 for **8a**, **8a**$^+$, and **8a**$^{2+}$, respectively, and 0.125, 0.750, and 0.125 for **8b**, **8b**$^+$, and **8b**$^{2+}$, respectively. These data indicate that the mixed-valence (MV) species are stable enough to predominate in solution, but in the determination of their molar properties, the presence of the associated neutral and dicationic complexes cannot be neglected.

The potential difference $\Delta E°$ and $K_c$ are often invoked as a measure of the electronic interaction through a given organic bridge for symmetrical compounds. This quantity is in fact related to the thermodynamic stability of the MV, for which energetic terms other than the one related to electronic interaction come into play.[3] For instance, through-space electronic interaction, solvation, entropy, or more specific factors, such as increased $\pi$-acidity in the MV state, steric interactions in the other redox states, and structural distortion upon oxidation, can influence its magnitude. Nevertheless, considering that the complexes **8a** and **8b** present very similar structural characteristics, one can assume that the values of $\Delta E°$ reflects *a weak electronic communication conveyed across the bonding between the remote metal centers*. Such communication can be probed only by the

(38) Klug, H. P.; Alexander, L. E. *X-Ray Diffraction Procedures*, 2nd ed.; John Wiley & Sons: New York, 1974.

Downloaded by NAT LIB UKRAINE on July 5, 2009
Published on April 20, 2004 on http://pubs.acs.org | doi: 10.1021/om034359i

spectroscopic observation of the IVCT band associated with the intramolecular electron transfer in the MV species. For this reason the synthesis of the oxidized species was carried out.

**4. Synthesis of 8a[PF$_6$]$_n$ and 8b[PF$_6$]$_n$ ($n$ = 1, 2).** As shown in Scheme 1, **8a** and **8b** were reacted with 1.95 equiv of [(C$_5$H$_4$)$_2$Fe][PF$_6$] in THF. Due to low stability of **8a**[PF$_6$]$_2$ and **8b**[PF$_6$]$_2$ in solution, the oxidation must be carried out following the procedure carefully. The solvent cooled at −80 °C was added to the solid reagents, and the mixture was stirred for 6 h at −80 °C. The complexes **8a**[PF$_6$]$_2$ and **8b**[PF$_6$]$_2$ were partially precipitated as pink powders (80−85%) by addition of cold pentane (−80 °C). As a solid, these complexes are air and thermally stable for several weeks. In solution, they slowly decompose in THF and much quicker in $CH_2Cl_2$ and $CHCl_3$. The salts **8a**[PF$_6$]$_2$ and **8b**[PF$_6$]$_2$, which show the same cyclic voltammograms as the parent compounds **8a** and **8b**, were characterized by IR, UV−vis, ESR, Mössbauer, and NIR spectroscopies.

The MV complexes **8a**[PF$_6$] and **8b**[PF$_6$] were not isolated. They were generated in situ by reacting the neutral complexes **8a** and **8b** with either an equivalent amount of [Cp$_2$Fe][PF$_6$] or **8a**[PF$_6$]$_2$ and **8b**[PF$_6$]$_2$. The spectroscopic measurements were repeated three times with freshly and independently prepared solutions, and the molar extinction coefficients were calculated using $K_c$ to determine the real concentration of all the species present in solution.

**5. Infrared Spectroscopy.** The IR spectra of the salts **8a**[PF$_6$]$_2$ and **8b**[PF$_6$]$_2$ present a low-energy absorption band characteristic of the PF bond stretch (Nujol ($CH_2Cl_2$), cm$^{-1}$) at 840 (839) and 838 (839) for **8a**[PF$_6$]$_2$ and **8b**[PF$_6$]$_2$, respectively. The spectra also display a single $\nu_{(C\equiv C)}$ stretching band at 2047 (2046) and 2046 (2046) for **8a**[PF$_6$]$_2$ and **8b**[PF$_6$]$_2$, respectively. Comparison of these IR data with those of the related neutral iron(II) species **8a** and **8b** shows that the oxidation produces a decrease in stretching frequency of the carbon−carbon triple bond of 35 and 34 cm$^{-1}$ for the compounds containing 3 and 4 methylene groups in the bridge, respectively. The lower stretching frequency observed in the oxidized compounds suggest a diminution of the bond order for the C≡C triple bond and, as a consequence, an increase of the bond order for the Fe(III)−C bonds. A weak contribution of an allenylidene-type resonance structure with a metal-centered or carbon-centered radical (forms **B1** and **B2** in Scheme 2) to the bonding description of this family of iron(III) complexes is in agreement with IR data[39] and DFT calculations[40] previously reported on related compounds. A degree of delocalization of the spin density on the $\beta$-carbon atom is also suggested by the weak chemical stability of these compounds in solution. Indeed, when **8a**[PF$_6$]$_2$ and **8b**[PF$_6$]$_2$ were kept in solution for a couple of hours, new bands appeared in the IR spectra around 1650 cm$^{-1}$, suggesting the formation of side products containing iron vinylidene groups, which possibly results from hydrogen atom abstraction from the solvent. A similar reaction was clearly established with the mononuclear complex [Cp*(dppe)Fe(C≡CH)][PF$_6$], which reacts with $CH_2Cl_2$ above −40 °C to yield [Cp*(dppe)Fe(=C=CH$_2$)][PF$_6$], quantitatively.[17] In contrast, it was shown that the iron(III) $\sigma$-alkynyl derivatives which bear a bulky group on the $\beta$-carbon atom are thermally stable.[24,25,40]

**Scheme 2**

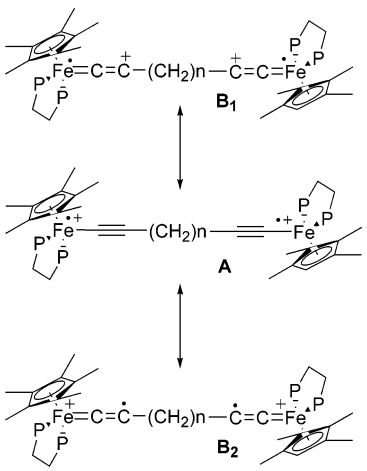


The MV complexes were also characterized by IR spectroscopy. The samples were in situ generated by addition of $CH_2Cl_2$ to an equimolecular mixture of the neutral and bis-oxidized compounds. The IR spectra were run both in solution and with a powdered sample obtained by evaporation of the solvent under vacuum. The IR spectra of the MV complexes **8a**[PF$_6$] and **8b**[PF$_6$] show two distinct $\nu$(C≡C) stretching bands. These bands are located at 2076 (2074) and 2037 (2037) in the spectrum of **8a**[PF$_6$], whereas they are seen at 2078 (2077) and 2039 (2039) in the case of **8b**[PF$_6$]. The vibration at higher frequency can be assigned to the $\nu$(C≡C) stretching mode of the Fe(II)−C≡C group, and the second absorption band corresponds to the Fe(III)−C≡C fragment. The presence of distinct absorption bands for the C≡C bond stretching provides evidence for localized oxidation states.

Comparison of these IR data with those found for the neutral and dications clearly shows that the electronic vacancy is located on one metal center, but also suggests a weak interaction between the Cp*(dppe)Fe−(C≡C)− building blocks through the bridge. Indeed, a shift to lower wavenumbers is observed for both the Fe(II)−C≡C and Fe(III)−C≡C vibrational modes. Relative to the corresponding homovalent iron(II) and iron(III) complexes, the decreases of the frequencies are 6 and 10 cm$^{-1}$ in the family of compounds with the −(C≡C)−(CH$_2$)$_3$−(C≡C)− bridge. As expected, this effect diminishes when the number of methylene groups in the linker increases. The frequencies decrease by 2 and 5 cm$^{-1}$ in the family of complexes **8b**[PF$_6$]$_n$. In the case of the weakly coupled MV complex **4**, the through-bridge metal−metal interaction was also probed by similar shifts of the $\nu$(C≡C) stretching modes.[20]

**6. $^{57}$Fe Mössbauer Data.** $^{57}$Fe Mössbauer spectroscopy is a powerful tool for the determination of the oxidation state of iron in organometallic complexes. The isomer shift ($\delta$) and the quadrupole splitting (QS) are very sensitive to the spin and oxidation states of the iron nucleus.[41,42] The $^{57}$Fe Mössbauer spectra of the

(39) Paul, F.; Mevellec, J.-Y.; Lapinte, C. *Dalton Trans.* **2002**, 1783.
(40) Weyland, T.; Costuas, K.; Mari, A.; Halet, J.-F.; Lapinte, C. *Organometallics* **1998**, *17*, 5569.

Downloaded by NAT LIB UKRAINE on July 5, 2009
Published on April 20, 2004 on http://pubs.acs.org | doi: 10.1021/om034359i

**Table 4. ESR Parameters for Compounds $8a^{n+}$ and $8b^{n+}$ ($n$ = 1, 2) and a Closely Selected Compound**

| cmpd | $g_1$ ($a_1$) | $g_2$ ($a_2$) | $g_3$ | $g_{iso}$[a] | $\Delta g$ |
|---|---|---|---|---|---|
| **8a**$^+$ | 1.981 (15 G) | 2.037 (12 G) | 2.433 | 2.150 | 0.452 |
| **8b**$^+$ | 1.979 | 2.037 | 2.438 | 2.151 | 0.459 |
| **9**$^{+}$[a] | 1.980 | 2.032 | 2.505 | 2.170 | 0.530 |
| **8a**$^{2+}$ | $\Delta m_s = \pm1$, $g = 2.2$, $\Delta H_{pp} = 600$ G; $\Delta m_s = \pm2$, $g = 4.267$ | | | | |
| **8b**$^{2+}$ | $\Delta m_s = \pm1$, $g = 2.2$, $\Delta H_{pp} = 700$ G; $\Delta m_s = \pm2$, signal not found | | | | |

[a] $g_{iso} = 1/3(g_1 + g_2 + g_3)$. [b] **9**$^+$ = [Cp*(dppe)FeC≡C−Bu$^t$][$PF_6$].[24]

complexes **8a**[$PF_6$]$_2$ ($\delta$ = 0.159 mm/s vs Fe, QS = 1.142 mm/s) and **8b**[$PF_6$]$_2$ ($\delta$ = 0.219 mm/s vs Fe, QS = 1.038 mm/s) recorded at zero field are characteristic of pure low-spin iron(III) and compare well with those of related mono- and polynuclear iron(III) compounds.[8,40,42] These values strongly differ from those obtained for the iron(II) complex **8b** ($\delta$ = 0.288 mm/s vs Fe, QS = 1.970 mm/s). More in-depth examination of the data shows a significantly smaller $\delta$ value for **8a**[$PF_6$]$_2$ than for **8b**[$PF_6$]$_2$, suggesting a lower electronic density at the iron nucleus for **8a**[$PF_6$]$_2$ than for **8b**[$PF_6$]$_2$. Such a difference could result from a better ligand −C≡C−$(CH_2)_x$−C≡C− to metal charge transfer in the ground state as the number of methylene groups and the interaction between the cationic metal centers decrease (form **B1** in Scheme 2). In addition, interactions between the cationic metal sites and the counteranions could also be considered to explain the Mössbauer spectra. Indeed, it is noteworthy that the Mössbauer response of the iron nucleus is affected by the nature of the counteranion. In particular, such a behavior was observed for the related complexes [Cp*(dppe)Fe{(=C)$_n$R$_2$}]X.[43] In addition, these two $Fe^{III}$ complexes possess QS parameters slightly larger than those usually found for $Fe^{III}$ derivatives of the same series, which range between 0.8 and 1.0 mm/s.[8,40,42] These values could be due either to the contribution of the canonical form **B1** or **B2** (Scheme 2, see above) in the description of the electronic structure of these complexes or to magnetic interactions between the paramagnetic metal centers.[43]

**7. ESR Measurements.** The low-temperature X-band ESR spectra of the dicationic complexes **8a**[$PF_6$]$_2$ and **8b**[$PF_6$]$_2$ show unresolved broad signals in a rigid glass (77 K, $CH_2Cl_2/C_2H_4Cl_2$, 1:1). As usually observed for biradicals,[40,44] the broadening of the signal is a consequence of electron−electron relaxation, which greatly shortens the relaxation time. The parameters (Table 4) compare well with those of other low-spin bis-iron(III) of the same series.[8] Moreover, a $\Delta m_s = \pm2$ transition characteristic of the triplet state is clearly observed at $g$ = 4.267 for the complex **8a**[$PF_6$]$_2$ (Figure 4) with a relative intensity of 1:85 for the $\Delta m_s = \pm1$ and $\Delta m_s = \pm2$ transitions.

The ESR spectra were run at 77 K in a rigid glass for samples of **8a**[$PF_6$] and **8b**[$PF_6$] generated by reacting in situ the neutral complex of **8a** and **8b** in the ESR tube with approximately 0.25 equiv of **8a**[$PF_6$]$_2$ and

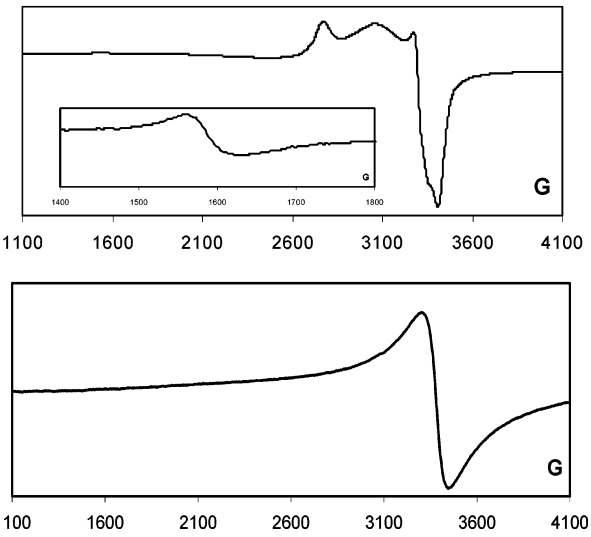


**Figure 4.** ESR spectra of **8a**[$PF_6$]$_2$ (top) and **8b**[$PF_6$]$_2$ (bottom) at 77 K.

**Table 5. UV−Vis NIR Absorption Data of Complexes $8a^n$+[$PF_6$]$_n$ and $8b^n$+[$PF_6$]$_n$ ($n$ = 0, 1, 2) in $CH_2Cl_2$ at 298 K**

| cmpd | absorption $\lambda_{abs}$/nm ($10^{-3}\epsilon$/ dm$^3$ mol$^{-1}$ cm$^{-1}$) |
|---|---|
| **8a** | 350 (4.4); 374 (3.9); 430 (2.8) |
| **8a**[$PF_6$] | 340 (5.5); 424 (2.8) |
| **8a**[$PF_6$]$_2$ | 340 (8.2); 426 (3.3) |
| **8b** | 350 (5.6); 374 (4.7); 430 (3.3) |
| **8b**[$PF_6$] | 340 (4.6); 416 (2.9) |
| **8b**[$PF_6$]$_2$ | 340 (8.2); 418 (2.5) |

**8b**[$PF_6$]$_2$. The spectra display three well-resolved features corresponding to the three components of the $g$ tensor as expected for $d^5$ low-spin $Fe^{III}$ in pseudooctahedral geometry.[24,45] The $g$ values extracted from the spectra are collected in Table 4. In the case of complex **8a**[$PF_6$], the resolution of the spectrum was good enough to observe the coupling with two phosphorus nuclei, indicating that the unpaired electron is located on a single metal center on the ESR time scale. For MV compounds of the Cp*(dppe)Fe series, it has been suggested that the anisotropy tensor ($\Delta g = g_1 - g_3$) decreases as the rate of the intramolecular electron transfer increases.[21] The $\Delta g$ values determined for both **8a**[$PF_6$] and **8b**[$PF_6$] are smaller than the value found for related mononuclear complexes and similar to the values reported for mixed-valence complexes with a small electronic coupling, suggesting that electron transfer occurs at a significant rate through the bonding for both mixed-valence complexes.

**8. UV−Vis Spectroscopies.** The electronic spectra of all the complexes **8a**[$PF_6$]$_n$ and **8b**[$PF_6$]$_n$ ($n$ = 0, 1, 2) show an intense high-energy band at 290 nm assigned to the intraligand $\pi \rightarrow \pi^*$ transitions and two or three low-energy bands of weaker intensity (Table 5). In the spectra of neutral complexes **8a** and **8b** three low-energy bands are observed, and upon one- or two-electron oxidation, the band at 374 nm disappears whereas the intensities of the two other bands increase. With reference to the related compound {Cp*(dppe)Fe(C≡C−$C_6H_5$)], which shows a low-energy absorption at 348 nm, the low-energy bands of **8a** and **8b** are tentatively

(41) Greenwood, N. N. *Mössbauer Spectroscopy*; Chapman and Hall: London, 1971.
(42) Guillaume, V.; Thominot, P.; Coat, F.; Mari, A.; Lapinte, C. *J. Organomet. Chem.* **1998**, *565*, 75.
(43) Argouarch, G.; Thominot, P.; Paul, F.; Toupet, L.; Lapinte, C. *C. R. Chim.* **2003**, *6*, 209.
(44) Paul, F.; Meyer, W. E.; Toupet, L.; Jiao, H.; Gladysz, J. A.; Lapinte, C. *J. Am. Chem. Soc.* **2000**, *122*, 9405.
(45) Rieger, P. H. *Coord. Chem. Rev.* **1994**, *135/136*, 203.

Downloaded by NAT LIB UKRAINE on July 5, 2009
Published on April 20, 2004 on http://pubs.acs.org | doi: 10.1021/om034359i

assigned to d$\pi$(Fe) → $\pi$*(C≡C) metal-to-ligand charge transfer (MLCT) transitions. It is likely that upon one-electron oxidation of the electron-rich $Fe^{II}$ center to $Fe^{III}$, the bands due to the d$\pi$(Fe) → $\pi$*(ligands) MLCT transition would vanish. As the intensities of the bands at 340 and 424 increase upon oxidation, one can assume that new bands ascribed to the ligand-to-metal charge transfer (LMCT) transition are located at this energy. In the related complex {Cp*(dppe)Fe(C≡C−$C_6H_5$)}[$PF_6$] the $\pi$(C≡C) → d$\pi$(Fe) LMCT transition is observed at lower energy (575 nm, 663 nm).[20] In the case of the complexes **8a**[$PF_6$]$_n$ and **8b**[$PF_6$]$_n$ ($n$ = 1, 2), the blue shift observed could be due to the restriction of the $\pi$-system to the akynyl fragments.

It is noteworthy that the UV−vis spectra of the MV complexes do not result from the simple addition of the spectra of the parent neutral and dication complexes. This observation indicates that the MV complexes cannot be regarded as bimetallic compounds constituted of two independent $Fe^{II}$ and $Fe^{III}$ sites, as already suggested by the IR and ESR spectroscopies.

**9. NIR Spectroscopy.** The spectra of the neutral complexes **8a** and **8b** do not contain any absorption bands in the NIR range. In contrast, the spectra of the homovalent $Fe^{III}$ diradical dications **8a**[$PF_6$]$_2$ and **8b**[$PF_6$]$_2$ contain a weak absorption band in the NIR range. These bands located at 5800 and 5810 $cm^{-1}$ for **8a**[$PF_6$]$_2$ and **8b**[$PF_6$]$_2$, respectively, have a weak intensity ($\epsilon$ = 50 ± 5 $M^{-1}$ $cm^{-1}$) and correspond to forbidden ligand field (LF) transitions specific for the Cp*(dppe)$Fe^{III}$ fragment.[46] Similar absorption bands were also observed in related chromium radicals.[47] In many cases, this iron(III) contribution is too weak to significantly affect the intense ICT band of $Fe^{II}$−$Fe^{III}$ mixed-valence compounds previously studied in this iron series,[18,48,49] but in the case where the intensity of the ICT band is also weak, the contribution of the LF transition must not be neglected.[20]

Bands were found in the NIR region for the two MV compounds **8a**[$PF_6$] and **8b**[$PF_6$]. These bands located on the tail of the LMCT transitions observed in the visible are broad, and their maxima are at 220 and 70 $M^{-1}$ $cm^{-1}$ for **8a**[$PF_6$] and **8b**[$PF_6$]$_2$, respectively (Figure 5). Assuming that the ICT bands have Gaussian profiles, the spectra of the MV complexes were deconvoluted in the range 3500−10000 $cm^{-1}$. The deconvolution procedure was carried out several times for spectra obtained with different samples and using different sets of parameters. As shown in Figure 5, the results show good agreement between the sum of the spectral components and the experimental spectra. For the complex **8a**[$PF_6$], the band shape analysis reveals the presence of three absorption bands in addition to the tail of the bands of the visible region. The parameters of the less intense and narrower band (A) fit very well with those of the LF transition observed for the homovalent $Fe^{III}$ dications (Table 6). The bands B and C are characteristic of the MV complex and should correspond to two different photoinduced electron transfer processes. The lower energy band (B) could be attributed to the superexchange (from $HOMO^{-1}$ to SOMO), whereas a transition from a lower energy level with a larger ligand character ($HOMO^{-n}$ ($n$ > 1) to SOMO) is observed at higher energy (band C).

The full widths at half-height ($\Delta\nu_{1/2}$) of the two bands are very close to the theoretical values derived from the NIR band position $\nu_{max}$ according to Hush's relationship for symmetrical MV complexes (see Table 6). For the MV complex **8b**[$PF_6$], the band shape analysis of the NIR spectrum shows only two bands. The lowest energy band could be safely attributed to LF transition. The other band, for which the experimental parameter $\Delta\nu_{1/2}$ is close to the theoretical value predicted by Hush's theory, should correspond to a $HOMO^{-n}$ to SOMO

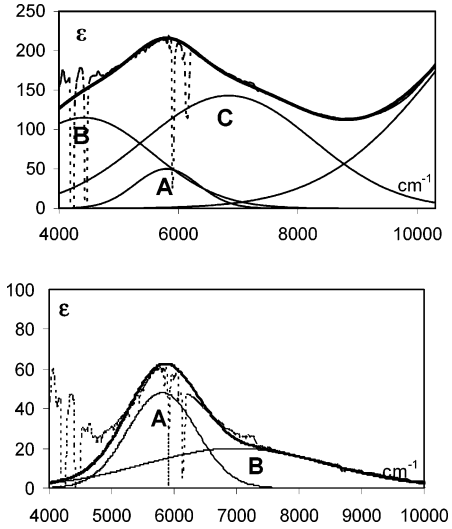


**Figure 5.** NIR spectra of **8a** (top) and **8b** (bottom) in $CH_2Cl_2$ [experimental (dashed lines), deconvoluted ICT bands (solid line), sum of the ICT components (bold line)].

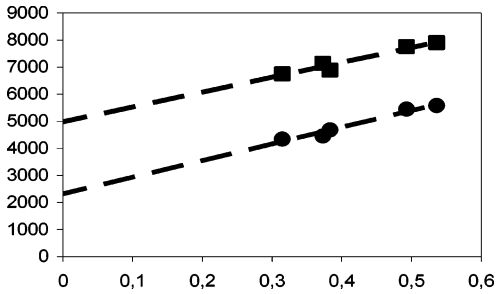

**Figure 6.** Plots of $E_{op}$ vs [$(1/n^2 - 1/D)$] for the NIR bands (B, circles; C, squares) of the MV complexes **8a**[$PF_6$].

**Table 6. Intervalence Charge Transfer Bands for 8a[$PF_6$] and 8b[$PF_6$]**

| cmpd | band | transition[a] | $\nu_{max}$ ($cm^{-1}$) | $\epsilon$ ($M^{-1}$ $cm^{-1}$) | $\Delta\nu_{1/2exp}$ ($cm^{-1}$) | $\Delta\nu_{1/2calc}$[b] ($cm^{-1}$) |
|---|---|---|---|---|---|---|
| **8a**$^+$ | A | LF | 5800 | 40 | 1500 | |
| | B | $HOMO^{-1}$ SOMO | 4680 | 110 | 3300 | 3290 |
| | C | $HOMO^{-n}$ SOMO | 6880 | 130 | 4000 | 3990 |
| **8b**$^+$ | A | LF | 5810 | 50 | 1560 | |
| | B | $HOMO^{-n}$ SOMO | 6990 | 20 | 4100 | 4020 |
| **4**$^+$ | A | LF | 5290 | 90 | 1450 | |
| | B | $HOMO^{-1}$ SOMO | 5540 | 310 | 3700 | 3600 |

[a] $n$ > 1. [b] $\Delta\nu_{1/2calc} = [2310\nu_{max}]^{1/2}$.

(46) Paul, F.; Lapinte, C. Work in progress.
(47) Atwood, C. G.; Geiger, W. E. *J. Am. Chem. Soc.* **1994**, *116*, 10849.
(48) Guillemot, M.; Toupet, L.; Lapinte, C. *Organometallics* **1998**, *17*, 1928.
(49) Paul, F.; Lapinte, C. Work in progress.

Downloaded by NAT LIB UKRAINE on July 5, 2009
Published on April 20, 2004 on http://pubs.acs.org | doi: 10.1021/om034359i

**Table 7. Near-Infrared Band Maxima for 8a[$PF_6$] as a Function of the Solvent**

| solvent | $1/n^{2a} - 1/D^b$ | band B ($cm^{-1}$) | band C ($cm^{-1}$) |
|---|---|---|---|
| 1,2-dichlorobenzene | 0.315 | 4350 | 6750 |
| THF | 0.373 | 4450 | 7140 |
| $CH_2Cl_2$ | 0.383 | 4680 | 6880 |
| Acetone | 0.493 | 5450 | 7750 |
| Methanol | 0.536 | 5580 | 7900 |

[a] $n$ is the refractive index. [b] $D$ is the static dielectric constant.

transition. Considering that the energy of this band is far from the energy found for the superexchange and very close to the energy of the $HOMO^{-n}$ to SOMO transition for **8a**[$PF_6$], it is possible that the superexchange does not take place across the spacer containing four methylene groups and only a more demanding energy process is observed.

The solvent dependence of the intervalence band maximum was investigated for the complex **8a**[$PF_6$]. Because compound **8b**[$PF_6$] is not soluble enough in polar solvents, this measurement could not be carried out for the latter. Due to the LF transition being weakly solvent sensitive,[46] the deconvolutions of the experimental spectra were performed in the range 3500−10000 $cm^{-1}$ assuming that band A is solvent independent. As the polarity of the solvent increases, the energy of both bands B and C at the maxima of absorption widely increases (Table 7). Hush's theory[50,51] of the effect of the solvent on the intervalence transition leads to eq 3, where $E_{outer}$ is the outer sphere Franck−Condon activation energy, $a_{FeIII}$ and $a_{FeII}$ are the diameters of dielectric saturation of the $Fe^{III}$ and $Fe^{II}$ centers, $d$ is the distance between the iron centers, $e$ is the electronic charge, $n$ is the refractive index,[52] and $D$ is the static dielectric constant[53] for a given solvent.[54]

$$E_{outer} = (1/a_{FeIII} + 1/a_{FeII} - 1/d)^{e^2}(1/n^2 - 1/D) \quad (3)$$

As shown from Figure 5, the energy of both bands B and C varies linearly (regression coefficients $R^2 = 0.99$) with $(1/n^2 - 1/D)$, as expected for intervalence transition in a weakly coupled system.[54−56] The two lines have very similar slopes, and their intercepts, which represent the Franck−Condon inner sphere optical activation energy ($\lambda_i$),[51] were found to be 2250 and 4800 $cm^{-1}$ for bands B and C, respectively. These values can be considered as moderate. They are significantly smaller than the $\lambda_i$ parameters determined for the compound $[(NH_3)_5Ru-L-Ru(NH_3)_5]^{5+}$ (L = 4,4′-bipy, $\lambda_i$ = 6290 $cm^{-1}$) and the famous Creutz and Taube complex (L = pyr, $\lambda_i$ = 5726 $cm^{-1}$).[55] The outer sphere reorganization energy is also weaker for **8a**[$PF_6$] than for the bis-ruthenium complex bridged with the 4,4′-bipyridine ligand ($\lambda_o$ = 3160 $cm^{-1}$).[54] Taken as a whole, the reorganization energies associated with the electron transfer for both MV complexes **8a**[$PF_6$] and **8b**[$PF_6$] are not large and are very close to the values found for the MV compound **4**[$PF_6$].[20] As a consequence, the diabatic energy surfaces corresponding to these MV complexes are flattened and the free energy of activation, $\Delta G^*$, is small (3.1 and 4.8 kcal/mol for **8a**[$PF_6$] and **8a**[$PF_6$], respectively) for the thermal electron transfer. This suggests that the electron transfer should be relatively rapid between the redox centers.

**Table 8. Characteristic Parameters for the Optical and Thermal Intramolecular Electron Transfer in the MV Complexes 8a[$PF_6$], 8a[$PF_6$], and the Closely Related Derivative 4[$PF_6$]**

| cmpd | $d_{Fe-Fe}$ (Å) | $E_{op}$ ($cm^{-1}$) | $\lambda_i$ ($cm^{-1}$) | $\lambda_o$[d] ($cm^{-1}$) | $\Delta G^{\ddagger}$ ($cm^{-1}$) | $V_{ab}$[e] ($cm^{-1}$) | $\alpha^2$[f] |
|---|---|---|---|---|---|---|---|
| **8a**[$PF_6$] | 8.50[b] | 4680 | 2250 | 2430 | 1170 | 110 | $4.9 \times 10^{-4}$ |
| | | 6880 | 4800 | 2080 | 1720 | 150 | $4.7 \times 10^{-4}$ |
| **8b**[$PF_6$] | 10[c] | 6990 | | | 1750 | 50 | $5.3 \times 10^{-5}$ |
| **4**[$PF_6$][a] | 10.2[b] | 5540 | | | 1385 | 160 | $8.9 \times 10^{-4}$ |

[a] From ref 20. [b] From X-ray powder diffraction diagram. [c] Estimated value. [d] From $\lambda = \lambda_i + \lambda_o$. [e] From $V_{ab} = 0.0205(\epsilon_{max}\nu_{max}\Delta\nu_{1/2})^{1/2}/(d_{Fe-Fe})$. [f] From $\alpha^2 = (V_{ab}/E_{op})^2$.

The electronic coupling parameter $V_{ab}$ can be calculated from the characteristics of the intervalence charge transfer band (Table 8). The $V_{ab}$ parameter obtained for **8a**[$PF_6$] is similar to the value previously determined for compound **4**[$PF_6$].[20] The value found for **8b**[$PF_6$] is much smaller, indicating that interaction between the metal centers decreases quickly with the number of methylene groups in the linker. These data compare well with those of an earlier work on MV complexes of the type $[(NH_3)_5Ru-S<>S-Ru(NH_3)_5][PF_6]$, where S<>S represents dithiaspiro ligands. In contrast with our flexible bridge, the dithiaspiro linker possesses a rigid and well-defined geometry. This comparison confirms that the geometry is not an overwhelming requirement for long-range electron transfer through fully saturated systems.[11,12] The α parameter, which represents the electronic delocalization, is weak, smaller than the value obtained for the complex **4**[$PF_6$], indicating that the spin density is localized on the iron atoms.

## Conclusion

The experimental data indicate that Hush's theory is well obeyed, as expected for weakly coupled MV. Analysis of the energetic parameters for the electron transfer between iron atoms in the MV complexes with the bridges $-C\equiv C-(CH_2)_n-C\equiv C-$ indicates that the presence of three or even four methylene groups in the $\pi$-electron system reduces the electronic communication between the remote redox-active centers, but nevertheless allows a surprisingly good through-bond interaction. This could be due, at least in part, to the weak reorganization energy associated with the oxidation/reduction of the iron centers. Moreover, it seems that the optically induced electron transfer occurs through two different pathways involving transition between the $HOMO^{-1}$/SOMO and $HOMO^{-n}$/SOMO orbitals. The overlap of these orbitals should provide continuous hyperconjugating electron transfer pathways between the iron atoms in accord with calculations previously reported for related MV ruthenium complexes.[12]

(50) Hush, N. S. *Prog. Inorg. Chem.* **1967**, *8*, 391.
(51) Hush, N. B. *Prog. Inorg. Chem.* **1971**, *8*, 391.
(52) Kosower, E. M. *An Introduction to Physical Organic Chemistry*; Wiley: New York, 1966; p 269.
(53) Weast, R. C. *Handbook of Chemistry and Physics*; Chemical Rubber Publishing Co: Cleveland, OH, 1969; p 154.
(54) Tom, G. M.; Creutz, C.; Taube, H. *J. Am. Chem. Soc.* **1974**, *96*, 7827.
(55) Powers, M. J.; Meyer, T. J. *J. Am. Chem. Soc.* **1980**, *102*, 1289.
(56) Creutz, C.; Taube, H. *J. Am. Chem. Soc.* **1969**, *91*, 3988.

Downloaded by NAT LIB UKRAINE on July 5, 2009
Published on April 20, 2004 on http://pubs.acs.org | doi: 10.1021/om034359i

Downloaded by NAT LIB UKRAINE on July 5, 2009
Published on April 20, 2004 on http://pubs.acs.org | doi: 10.1021/om034359i

## Experimental Section

**General Data.** All the manipulations were carried out under an argon atmosphere using Schlenk techniques or in a Jacomex 532 drybox filled with nitrogen. Routine NMR spectra were recorded using a Bruker DPX 200 spectrometer. High-field NMR spectral experiments were performed on a multinuclear Bruker WB 300 instrument. Chemical shifts are given in parts per million relative to tetramethylsilane (TMS) for $^1$H and $^{13}$C NMR spectra, and $H_3PO_4$ for $^{31}$P NMR spectra. X-Band ESR spectra were recorded on a Bruker ESP-300E spectrometer. An Air Products LTD-3-110 liquid helium transfer system was attached for the low-temperature measurements. The $^{57}$Fe Mössbauer spectra were obtained by using a constant acceleration spectrometer previously described with a 50 mCi $^{57}$Co source in a Rh matrix. The sample temperature was controlled by a Oxford MD306 cryostat and a Oxford ITC4 temperature controller. Computer fitting of the Mössbauer data to Lorenzian line shapes was carried out with a previously reported computer program. The isomer shift values are reported with respect to iron foil at 298 K and are not corrected for the temperature-dependent second-order Doppler shift. The Mössbauer sample cell consists of a 2 cm diameter cylindrical Plexiglas holder. Elemental analyses were performed at the Centre de Microanalyses du CNRS, Lyon-Solaise, France.

**[Cp*(dppe)Fe=C=C(H)(CH$_2$)$_3$(H)C=C=Fe(dppe)Cp*][BPh$_4$]$_2$ (7a)**. A Schlenk tube was charged with Cp*(dppe)FeCl (**6**, 0.500 g, 0.80 mmol), $NaBPh_4$ (0.274 g, 0.80 mmol), 40 mL of methanol, and a magnetic stir bar. Then hepta-1,6-diyne (39 $\mu$L, 0.33 mol) was added. The reaction mixture, which was stirred for 36 h, gradually turned orange. The solvent was removed under vacuum and the residue extracted with 2 × 30 mL of $CH_2Cl_2$. After concentration (to 10 mL) an orange solid was precipitated by addition of 100 mL of pentane. The suspension was filtered off, washed with pentane (2 × 20 mL), and dried under vacuum. The compound **7a** was recovered as an air-stable orange powder (0.611 g, 97%). FTIR (Nujol/$CH_2Cl_2$, cm$^{-1}$): $\nu$ 1645/1644 (s, C=C). $^1$H NMR (200 MHz, $CDCl_3$): $\delta$ 7.45−6.84 (m, 80H, $C_6H_5$), 3.99 (t, 2H, $^4J_{PH}$ = 3.8 Hz, C=CH), 2.51−2.14 (2m, 8H, $CH_{2dppe}$), 1.44−0.71 (2m, 6H, $CH_2$), 1.42 (s, 30H, Cp*). $^{13}$C NMR (50 MHz, $CDCl_3$): $\delta$ 354.4 (t, $^2J_{CP}$ = 33 Hz, C$_\alpha$), 166.1−122.1 (m, Ph); 119.9 (d, $^1J_{CH}$ = 152 Hz, C$_\beta$), 99.6 (s, $C_5Me_5$), 34.2 (m, $^1J_{CH}$ = 131 Hz, $CH_2$), 29.9 (tm, $^1J_{CP}$ = 23 Hz, $CH_{2dppe}$), 21.2 (m, $^1J_{CH}$ = 133 Hz, $CH_2$), 10.5 (q, $^1J_{CH}$ = 128.7 Hz, $C_5Me_5$). $^{31}$P{$^1$H} NMR (81 MHz, $CDCl_3$, 25 °C, $H_3PO_4$ ext): $\delta$ 90.5 (s, dppe). MS (positive LSI, o-NPOE): *m*/*z* 1589.6 (M$^+$, 3%), 589.3 ([Cp*(dppe)Fe]$^+$, 33%). HRMS [C$^{2+}$, $BPh_4^-$]$^+$: *m*/*z* calc 1589.6037, found 1589.6064.

**[Cp*(dppe)Fe=C=C(H)(CH$_2$)$_4$(H)C=C=Fe(dppe)Cp*][BPh$_4$]$_2$ (7b).** Following the procedure described for **7a**, complex **7b** was prepared and isolated as an orange powder (0.620 g, 96%) by reacting **6** with octa-1,7-diyne (45 $\mu$L, 0.33 mmol). IR (Nujol, cm$^{-1}$): $\nu$ 1648 (s, C=C). $^1$H NMR (200 MHz, $CDCl_3$): $\delta$ 7.70−6.82 (m, 80H, $C_6H_5$), 4.06 (t, 2H, =CH, $^4J_{PH}$ = 3.8 Hz), 2.54−2.15 (2m, 8H, $CH_2$dppe), 1.44−0.75 (2m, 8H, $CH_2$), 1.42 (s, 30H, Cp*). $^{31}$P{$^1$H} NMR (81 MHz, $CDCl_3$): $\delta$ 90.6 (s, dppe). $^{13}$C NMR (50 MHz, $CDCl_3$): $\delta$ 354.8 (t, $^2J_{CP}$ = 33 Hz, C$_\alpha$), 166.1−122.1 (m, Ph), 120.0 (d, $^1J_{CH}$ = 152 Hz, C$_\beta$), 99.5 (s, $C_5Me_5$), 30.6 (m, $^1J_{CH}$ = 131 Hz, $CH_2$), 29.7 (tm, $^1J_{CP}$ = 23 Hz, $CH_{2dppe}$), 21.0 (m, $^1J_{CH}$ = 133 Hz, $CH_2$), 10.4 (q, $^1J_{CH}$ = 128.7 Hz, $C_5Me_5$).

**Cp*(dppe)FeC≡C(CH$_2$)$_3$C≡CFe(dppe)Cp* (8a).** To a solution of **7a** (0.530 g, 0.28 mmol) in THF (40 mL) was added KO$^t$Bu (0.075 g, 0.67 mmol). The resulting brown-orange solution was stirred for 4 h at 20 °C and evaporated to dryness in vacuo. The crude residue was extracted with toluene (4 × 20 mL), the resulting solution concentrated to 5 mL, and pentane added to precipitate the salts (50 mL). After filtration and evaporation to dryness in vacuo, compound **8a** was obtained as an air-stable orange powder (0.315 g, 90%). Anal. Calcd for $C_{79}H_{84}Fe_2P_4$: C 74.77, H 6.67. Found: C 74.13, H 6.65. FTIR (Nujol/$CH_2Cl_2$, cm$^{-1}$): $\nu$ 2082/2080 (s, C≡C). $^1$H NMR (200 MHz, $C_6D_6$): $\delta$ 8.08−6.99 (m, 40H, $C_6H_5$), 2.79−1.94 (2m, 8H, $CH_{2dppe}$), 2.53−1.72 (2m, 6H, $CH_2$), 1.57 (s, 30H, Cp*). $^{31}$P{$^1$H} NMR (81 MHz, $C_6D_6$): $\delta$ 102.8 (s, dppe). $^{13}$C NMR (50 MHz, $C_6D_6$, 25 °C, TMS ext): $\delta$ 141.0−127.0 (m, Ph), 117.1 (s, C$_\beta$), 108.7 (t, $^2J_{CP}$ = 41 Hz, C$_\alpha$), 87.2 (s, $C_5Me_5$), 33.6 (tm, $CH_2$), 31.2 (tm, $^1J_{CP}$ = 22 Hz, $CH_{2dppe}$), 24.2 (tm, $CH_2$), 10.7 (q, $^1J_{CH}$ = 127 Hz, $C_5Me_5$). MS (positive LSI, o-NPOE): *m*/*z* 1268.4 (M, 13%), 589.3 ([Cp*Fedppe]$^+$, 39%). HRMS *m*/*z* calc 1268.4222, found 1268.4226.

**Cp*(dppe)FeC≡C(CH$_2$)$_4$C≡CFe(dppe)Cp* (8b).** As described for the preparation of **8a**, a solution of **7b** (1.240 g, 0.645 mmol) in THF (40 mL) was treated with KO$^t$Bu (0.174 g, 1.56 mmol). Compound **8b** was isolated as a red-orange powder (0.761 g, 92%). FTIR (Nujol/$CH_2Cl_2$, cm$^{-1}$): $\nu$ 2080/2080 (s, C≡C). $^1$H NMR (200 MHz, $C_6D_6$): $\delta$ 8.07−7.09 (m, 40H, $C_6H_5$), 2.68−1.88 (2m, 8H, $CH_{2dppe}$), 2.54−1,27 (2m, 8H, $CH_2$), 1.56 (s, 30H, Cp*). $^{13}$C NMR (50 MHz, $C_6D_6$): $\delta$ 140.9−127.0 (m, $C_6H_5$), 117.0 (t, $^3J_{Cp}$ = 3 Hz, C$_\beta$), 109.1 (t, $^2J_{CP}$ = 41 Hz, C$_\alpha$), 87.2 (s, $C_5Me_5$), 31.2 (tm, $^1J_{CP}$ = 22 Hz, $CH_{2dppe}$), 24.2 (tm, $^1J_{CH}$ = 126 Hz, $CH_2$), 10.7 (q, $^1J_{CH}$ = 128 Hz, $C_5Me_5$). $^{31}$P-{$^1$H} NMR (81 MHz, $C_6D_6$): $\delta$ 102.6 (s, dppe). MS (LSIMS+, *m*-NBA): *m*/*z* 1283,4 (M + H, 7%); 589,2 (Cp*(dppe)Fe, 100%). HRMS *m*/*z* calc 1282.4379, found 1283.4375.

**[Cp*(dppe)FeC≡C(CH$_2$)$_3$C≡CFe(dppe)Cp*][PF$_6$]$_2$ (8a[PF$_6$]$_2$)**. To **8a** (0.200 g, 0.157 mmol) and [$FeCp_2$][$PF_6$] (0.102 g, 0.307 mmol) was added THF (20 mL) at −80 °C. The solution was stirred for 6 h, then cold pentane (−80 °C, 100 mL) was added. A pink powder precipitated from the solution. This powder was isolated by filtration and washed with diethyl ether (3 × 20 mL) and pentane (2 × 30 mL) at −80 °C. After drying under vacuum, the powder was allowed to warm to 20 °C. The air and thermally stable solid was identified as **8a**[$PF_6$]$_2$ (0.195, 80%). FTIR (Nujol/$CH_2Cl_2$, cm$^{-1}$): $\nu$ 2047/2046 (s/m, C≡C), 840/839 (s, PF).

**[Cp*(dppe)FeC≡C(CH$_2$)$_4$C≡CFe(dppe)Cp*][PF$_6$]$_2$ (8b[PF$_6$]$_2$)**. Complex **8b**[$PF_6$]$_2$ was obtained (0.400 g, 85%) by reacting **8b** (0.380 g, 0.296 mmol) with [$FeCp_2$][$PF_6$] (0.191 g, 0.577 mmol) following the procedure used to prepare **8a**[$PF_6$]$_2$. FTIR (Nujol/ $CH_2Cl_2$, cm$^{-1}$): $\nu$ 2047/2046 (s/m, C≡C), 840/839 (s, PF).

**Single-Crystal X-ray Data Collection and Structure Determination for 8a.** A crystal of **8a** was glued to a glass fiber mounted on a four-circle Nonius Kappa CCD area-detector diffractometer. Intensity data sets were collected using Mo K$\alpha$ radiation through the program COLLECT.[57] Correction for the Lorentz−polarization effect, peak integration, and background determination were carried out with the program DENZO.[58] Frame scaling and unit cell parameter refinement were performed with the program SCALEPACK.[58] Analytical absorption corrections were performed by modeling the crystal faces using NUMABS.[59] The structure was solved with the triclinic space group $P\bar{1}$. Iron and phosphorus atoms were located using the direct methods with the program SIR97.[60] The complete model was found from successive Fourier calculations using SHELXL-97.[61] All H atoms were generated and refined using the "riding" option available in SHELXL-97.

**X-ray Powder Diffraction for 8a.** Powder diffraction data of **8a** were collected with a Bruker D5005 diffractometer using

(57) Nonius *Kappa CCD Software*; Nonius BV: Delft, The Netherlands, 1999.
(58) Otwinowski, Z.; Minor, W. Processing of X-ray Diffraction Data Collected in Oscillation Mode. In *Methods in Enzymology, Macromolecular Crystallography*, Carter, C. W., Sweet, R. M., Eds.; Academic Press: New York, 1997; Vol. 276, Part A, p 307.
(59) Coppens, P. In *Crystallographic Computing*; Munksgaard Publishers: Copenhagen, 1970.
(60) Altomare, A.; Burla, M. C.; Camali, M.; Cascarano, G.; Giacovazzo, C.; Guagliardi, A.; Moliterni, A. G. G.; Polidori, G.; Spagna, R. *J. Appl. Crystallogr.* **1999**, *31*, 115.
(61) Sheldrick, G. M. *SHELX97. Program for Refinement of Crystal Structures*; University of Göttingen: Göttingen, Germany, 1997.

Cu Kα radiation ($\lambda$(Kα1) = 1.5406 Å, $\lambda$(Kα2) = 1.5444 Å) selected with a diffracted-beam graphite monochromator. The data were collected over the angular range 3.00−60.00° ($2\theta$) (step length 0.04° ($2\theta$), counting time 35 s step$^{-1}$). The extraction of peak positions was carried out with the Socabim fitting program, available in the software package DIFFRACplus supplied by Bruker AXS.

**Acknowledgment.** We thank A. Mari (LCC, Toulouse) for Mössbauer measurements. L.C. and S.R. are indebted to ANRT and Laboratoires Standa (Caen) for financial support and a thesis grant to S.R. We are indebted to Drs. D. Louer and P. Hapiot (Rennes) for stimulating discussions.

**Supporting Information Available:** Simulated CVs of **8a** and **8b** and crystallographic data for compound **8a**. This information is available free of charge via the Internet at http://pubs.acs.org.

OM034359I

Downloaded by NAT LIB UKRAINE on July 5, 2009
Published on April 20, 2004 on http://pubs.acs.org | doi: 10.1021/om034359i